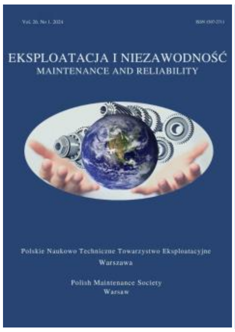

Eksploatacja i Niezawodnosc – Maintenance and Reliability
Volume 26 (2024), Issue 1
journal homepage: http://www.ein.org.pl

Article citation info:
Zhang J, Lu H, Jiang H, Miao Y, Shi Z, Study on reliability of emergency braking performance of high-speed and heavy-load monorail crane, Eksploatacja i Niezawodnosc – Maintenance and Reliability 2024: 26(1) http://doi.org/10.17531/ein/174820

Study on reliability of emergency braking performance of high-speed and heavy-load monorail crane

Indexed by: Web of Science Group

Jiarong Zhang[a], Hao Lu[a,b,*], Hui Jiang[a], Yun Miao[a], Zhiyuan Shi[c]

[a] School of Mechatronic Engineering, China University of Mining and Technology, China
[b] Jiangsu Key Laboratory of Mine Mechanical and Electrical Equipment, China University of Mining and Technology, China
[c] China Mining Products Safety Approval and Certification Center, China

Highlights

- The random response of braking performance is obtained by combining LHS and DD.
- High-order moment saddlepoint approximation is used to estimate the failure probability.
- Reasonable selection of relevant parameters is important for braking safety.
- The failure modes of monorail crane mainly include braking distance failure and braking temperature failure.

Abstract

The reliability of monorail crane braking system has an important influence on the braking safety. The high speed and heavy load operation poses a great challenge to the braking safety, and it is necessary to evaluate its braking reliability accurately and efficiently. Firstly, the dynamic performance and thermal-mechanical coupling characteristics of high-speed and heavy-load monorail crane under different braking parameters were analyzed. Secondly, the random response model of braking distance and braking temperature was established by combining the design of experiment method (DoE) and Dendrite Net (DD). Finally, the high-order moment saddlepoint approximation (SPA) method was used to evaluate the emergency braking reliability of the monorail crane. The results can provide a reference for the selection of key parameters and the evaluation of braking safety of the monorail crane braking system under high-speed and heavy-load conditions.

Keywords
monorail crane, braking system, reliability, surrogate model

1. Introduction

Monorail crane is an important form of underground auxiliary transportation equipment with high transport efficiency and high mobility. Figure 1 shows the structural components of a monorail crane. In recent years, with the increasing demand for transportation efficiency in underground coal mining, the requirements for emergency braking performance of monorail cranes in high-speed, heavy-load downhill conditions are very strict. Therefore, reliability evaluation of the braking system is of great significance for improving mine production safety and reducing the occurrence of malignant accidents.

The braking system reliability has been studied from several aspects. In the reliability analysis of the thermal-mechanical coupling failure of brakes, Ren et al. [25] used Kriging model to establish the relationship between random variables and brake shoe temperature and stress, evaluated the reliability of the braking system considering multi-failure modes through Copula function. Dammak et al. [3] used Kriging model to carry out reliability-based robust optimization design (RBROD) on the basis of brake disc structure and temperature rise analysis. Yang et al. [28] used AK-MCS to develop a performance

(*) Corresponding author.
E-mail addresses: J. Zhang 03180866@cumt.edu.cn, H. Lu (ORCID: 0000-0002-5188-1624) haolu@cumt.edu.cn, H. Jiang 2448646465@qq.com , Y. Miao miaoyun000101@163.com , Z. Shi shizhiyuancumt@126.com

function model for the thermal-mechanical coupling reliability of drum brakes and carried out reliability optimization design.

Regarding the issue of vibration failure in brakes, Zhang et al. [32] conducted reliability analysis of brake shoes considering random strength degradation, and the reliability of brake shoes was predicted for different impact load frequencies and initial strengths. Yang et al. obtained sample data between drum brake design parameters and natural frequencies by DoE method [30], and carried out vibration reliability by BP neural network, radial basis function neural network with important sampling method (RBF-IS) [29]. To address the problem of squeal instability of automotive brakes, Lyu et al. [21,22] proposed the random and fuzzy model and the fuzzy random model for the squeal instability reliability analysis of automotive brake discs, and proposed an interval variable-based response surface method (RSM) to approximate the implicit relationship between the approximation system parameters and noise modes.

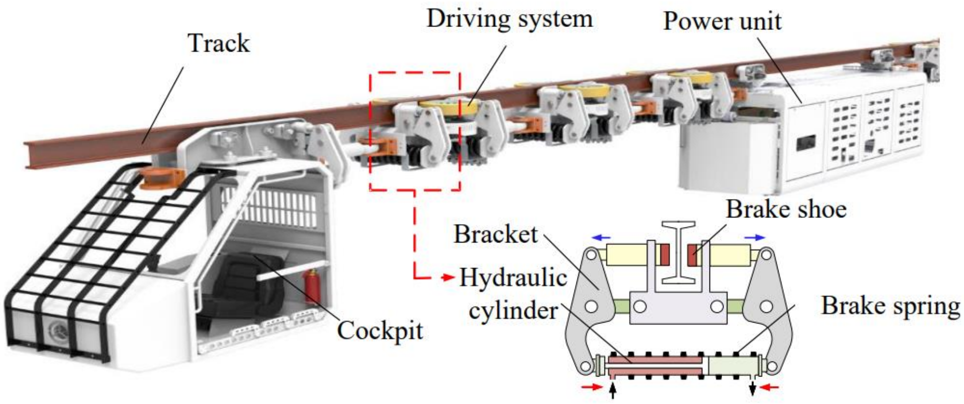

Fig.1. Structural components of a monorail crane.

For certain complex structural systems, the relationship between the input and output of random variables may be highly non-linear, occasionally implicit expressions. In cases where the reliability analysis model cannot be determined directly, the use of surrogate models to approximate complex systems can save significant computational resources and time. Polynomial RSM [8] approximates implicit functions by combination of the polynomial functions (mainly linear and quadratic) of the input variables, and several improved RSM methods have been developed in recent years, such as the high-order stochastic response surface method (HO-SRSM) [18], RSM based on projective dimensionality reduction techniques, [9] etc. The Kriging model [17] refers to a surrogate model based on Gaussian process modelling, improved Kriging models include Monte Carlo simulation with an active learning Kriging model (AK-MCS) [7], Kriging model method based on dimensionality reduction techniques [34], composite Kriging models [13]. In addition, there are artificial neural networks (ANN) [4,27], least squares support vector machine (LS-SVM) [12], polynomial chaos expansion (PCE) [1,23], ensemble of surrogates [2,24] and other methods.

In the estimation of the failure probability of the system, the SPA method can be used to approximate the properties of a performance function because of its good approximation to small probability failure problems. Tvedt [26] applied SPA to the second-order reliability method (SORM). Du et al. [5,6] proposed the first-order saddlepoint approximation (FOSPA) method to solve the non-linear problem caused by the transformation of the standard normal space of random variables, which first linearizes the performance function and then approximates its PDF using SPA. In addition to deriving an approximate performance function using a Taylor expansion of the limit state function at the Most Likelihood Point (MLP), an approximate cumulative generating function (CGF) for the performance function can be constructed based on statistical moments and then approximated its cumulative distribution function (CDF) using SPA [11]. Zhou et al. [33] used an adaptive trivariate dimensional decomposition method to calculate the first six-order moments of the performance function, SPA method based on the first six-order moments was proposed to estimate the failure probability of the system for its high accuracy and validity. Huang et al. [14,16] used SPA and dimension reduction method to estimate the CDF and PDF of the response, which showed a higher accuracy than the traditional first-order and second-order reliability methods. Guo et al. [10] proposed a third-order moment SPA technique that does not strictly require the CGF of the random variables, the third-order moment SPA method can be used for reliability assessment whether or not the PDF of the random variables is known. Furthermore, the reliability-based interdisciplinary design optimization can be performed using the proposed third-order moment SPA [31].

Considering the complex transportation conditions, high-speed and heavy-load monorail cranes often face emergency braking. The high stress and temperature caused by the friction between the brake shoe and the track have a significant impact on the operational stability of the brake. Therefore, studying the reliability of emergency braking performance of high-speed and heavy-load monorail cranes is of great significance. This paper takes the braking system of DC200/105Y explosion-proof diesel monorail crane as the research object, aims at carrying out the reliability modelling and evaluation of the braking system from two aspects of braking distance and braking temperature. The remaining part of the paper is organized as follows. In Section 2, the influence of relevant parameters on the dynamic and thermal-mechanical coupling characteristics of the braking system is obtained through FEA. In Section 3, a DD random response model for the emergency braking characteristics is presented for braking distance and temperature failure modes. In Section 4, the CDF of the performance function is approximated using high-order moment SPA method and reliability calculation is carried out. Several conclusions are given in the last section.

2. Analysis of the factors influencing the braking performance

The three-dimensional model of the monorail crane braking system is established, as shown in Figure 2. In the non-braking state, the brake hydraulic cylinder is filled with oil to compress the brake spring. At the same time, the brake bracket compresses the brake shoes onto the track, making it possible to maintain a safe clearance between the brake shoe and the track. In the braking state, the brake cylinder is unloaded through the hydraulic control valve, the brake spring returns under the action of the preload and drives the brake shoes to hold the track tightly until it is completely stopped.

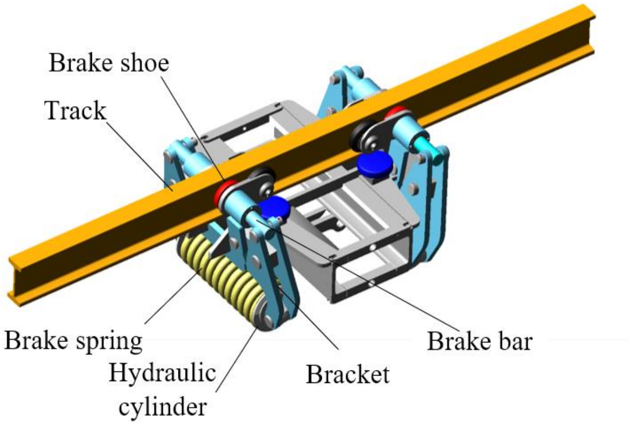

Fig. 2. Finite element model of the braking system.

The braking distance and braking speed, as important indicators of the dynamic performance of the braking system, have a significant impact on braking efficiency and safety. At the same time, during the emergency braking process of the braking system, there is a sharp rise in the surface temperature of the brake shoe due to the brake pressure on the track, seriously affecting the transportation safety and efficiency of the monorail crane. Therefore, it is necessary to carry out a thermal-mechanical coupling analysis under emergency braking conditions.

In this section, the temperature and stress fields distribution of the brake shoe are analyzed. In addition, the influence laws of important system parameters on the dynamic and thermal-mechanical coupling characteristics of the brake shoe are considered, which is a parameter selection basis for further reliability modeling.

2.1. Dynamic characteristics analysis of the brake shoe

The three-dimensional model of the monorail crane braking system is imported into ADAMS for dynamics simulation analysis. The effect of spring stiffness, braking clearance, and friction coefficient on the braking performance is investigated when braking on a vertical curved track with a radius of 10m at an initial speed of 2.6m/s and a load of 48 tons.

2.1.1. Factors influencing dynamic characteristics

The brake spring is the core component of the braking system and it has an important effect on braking performance of the monorail crane. With the increase in braking frequency and running time, the stiffness of brake spring will undergo a certain degree of deterioration under the influence of manufacturing techniques, alternate loads, and a corrosive environment.

Considering the complex working environment of underground coal mines, monorail crane transport routes are usually set up with many curves. According to the "Coal Industry Standard MT933-2005", the radius of the track cannot be less than 4m to satisfy the normal operation of the monorail crane. Therefore, there must be a certain braking clearance between the brake shoe and the track. The braking clearance of the research object is set as 10mm. It is worth mentioning that, a large amount of heat is generated on the friction surface due to the high braking pressure during the actual braking process, resulting in severe wear on the brake shoe surface. The braking clearance becomes larger leading to insufficient braking force, which poses a great threat to the braking safety of the monorail crane.

When the brake pressure is constant, the friction coefficient is the main factor affecting the braking force. There are two main reasons for the change in the friction coefficient of the sliding friction pairs. Firstly, the surface material will undergo changes in physical properties under the effect of frictional wear. Secondly, dust accumulation, a moist environment and oil pollution can also lead to a lower friction coefficient, which will affect the braking performance of the monorail crane.

On the basis of actual condition, spring stiffnesses of 113N/mm, 124N/mm, 135N/mm, and 146N/mm, braking clearance of 7mm, 11mm, 15mm, and 19mm, friction coefficient of 0.29, 0.32, 0.35, and 0.38 are selected for simulation.

2.1.2. Analysis of the variation trend in braking distance and speed

In order to explore the influence of the above three factors on the braking distance and speed, FEA was carried out and the results are shown in the figures below.

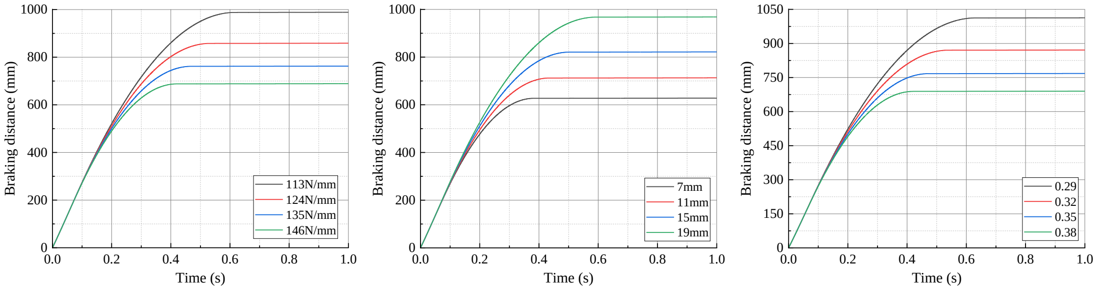

(a) (b) (c)

Figure 3 Variation of braking distance for different factors

(a) Braking distance curve as spring stiffness changes

(b) Braking distance curve as braking clearance changes

(c) Braking distance curve as friction coefficient changes

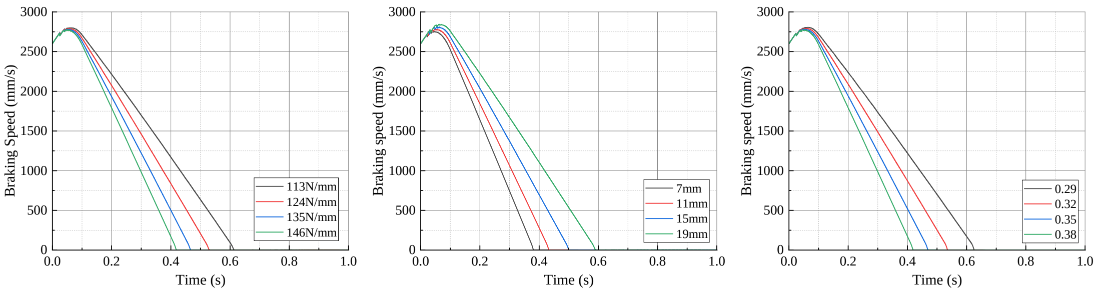

(a) (b) (c)

Figure 4 Variation of braking speed for different factors

(a) Braking speed curve as spring stiffness changes

(b) Braking speed curve as braking clearance changes

(c) Braking speed curve as friction coefficient changes

It can be seen from the Figures that the emergency braking distance of the monorail crane changes significantly when each factor changes. The speed of the monorail crane first increases from 2.6 m/s until it reaches a certain value, then gradually decreases to 0m/s. The monorail crane did not slow down immediately because of the presence of the brake clearance, during which the monorail crane receives no braking resistance.

As the spring stiffness and friction coefficient increase, the braking distance and braking time decrease. Conversely, an increase in braking clearance leads to an increase in both the braking distance and braking time. Furthermore, it is noteworthy that a larger spring stiffness results in a slower rate of decrease in the braking distance and braking time.

Therefore, the braking performance of the monorail crane can be improved by reasonably increasing the brake spring stiffness and friction coefficient of materials, or reducing braking clearance.

2.2. Thermal-mechanical coupling analysis of the brake shoe

In this section, the distribution of the stress and temperature fields in the brake shoe under emergency braking conditions is investigated. The three-dimensional model of the braking system is imported into ABAQUS to conduct the thermal-mechanical coupling analysis.

To make the simulation process closer to the actual braking conditions, the following conditions are made for the finite element model of the monorail crane brake. The working load of the monorail crane braking system is 48 tons, running on a downhill track with a gradient of 30°. Based on the heat conduction theory, it can be calculated that during the braking process, 54.5% of the heat generated by friction is transferred to the brake shoe and 45.5% is transferred to the track. Moreover, the braking parameters under emergency braking conditions have been obtained and are presented in Table 1.

Table 1 The parameters for emergency braking conditions of the monorail crane

Parameter Names	Value
Initial speed (m/s)	2.6
Braking pressure (MPa)	13
Friction coefficient	0.38
Braking clearance (mm)	10
Environment temperature (°C)	20
Brake shoe radius (mm)	35
Brake shoe thickness (mm)	10

2.2.1. Analysis of brake shoe temperature and stress fields distribution

The monorail crane experiences intense friction between the brake shoe and the track during the emergency braking process, resulting in a rapid heat accumulation in the brake shoes. The uneven distribution of temperature on the surface of the brake shoe can lead to uneven thermal stress distribution, leading to thermal cracks in specific locations, which can affect the working life and braking performance of the system. Therefore, it is necessary to study the temperature and stress fields of the brake shoe.

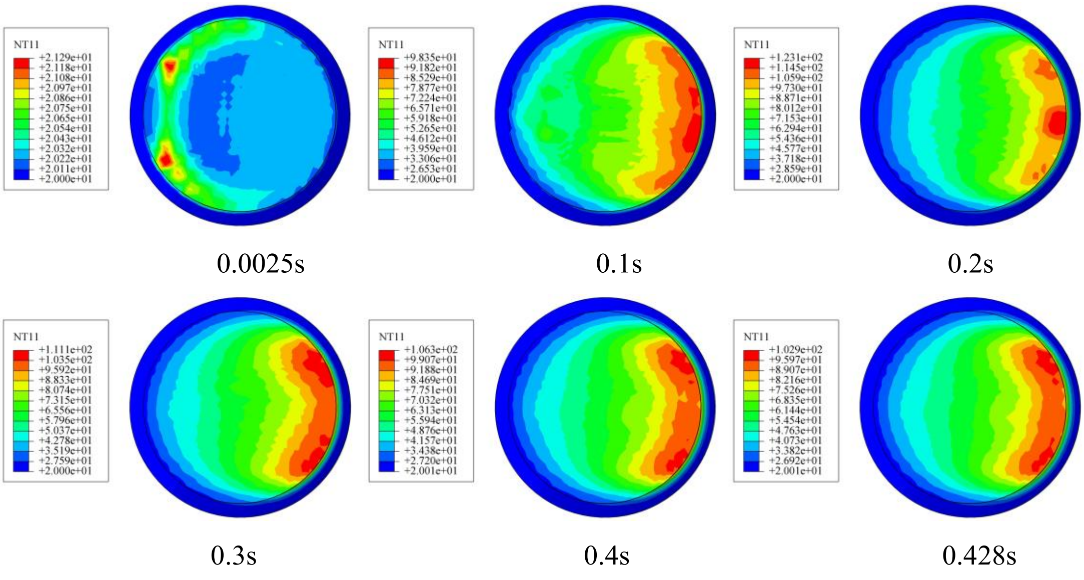

Fig. 5. The temperature field distribution of the brake shoe at different braking times.

Figure 5 shows the temperature field distribution of the brake shoe during the emergency braking process at different braking times, it is evident that the surface temperature of the brake shoe exhibits an axisymmetric distribution along the direction of motion.When the brake shoe initially contacts with the track, the heat primarily accumulates on the front side of the brake shoe in relation to the motion direction, exhibiting a semi-circular distribution pattern. As the braking pressure and braking time increase, the surface temperature of the brake shoe gradually rises. Moreover, the heat progressively accumulates in the region opposite to the motion direction, resulting in a more significant area of high temperature. The low-temperature area primarily concentrates at the edge of the friction surface. This occurs due to its extensive contact area with the external environment, allowing for relatively efficient heat dissipation.

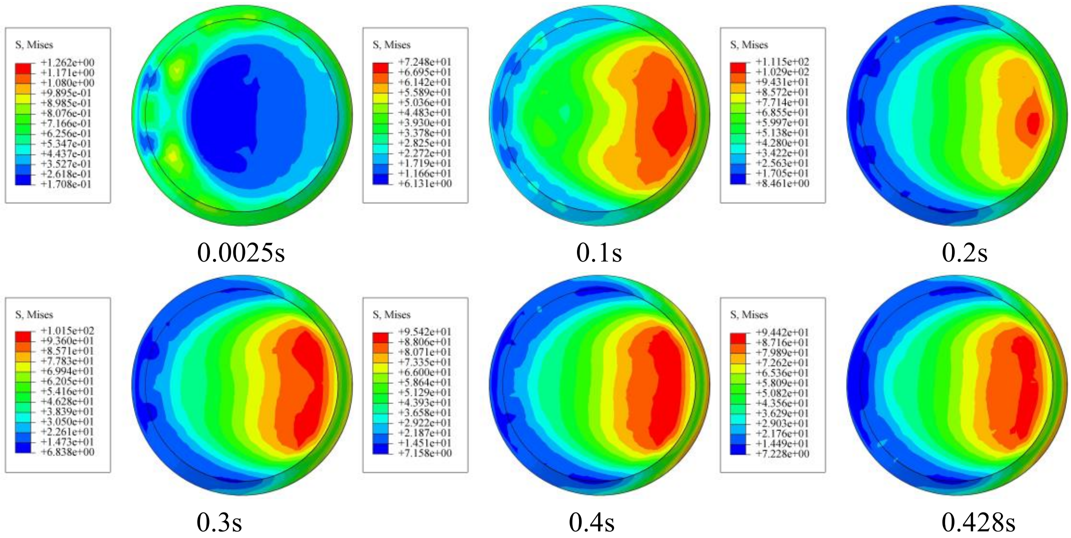

Fig. 6. The stress field distribution of the brake shoe at different braking times.

The stress field distribution of different braking times under emergency braking conditions of the brake shoe is shown in Figure 6. The figure reveals that the initial stress during braking primarily concentrates on the front side of the brake shoe in relation to the motion direction. As the braking time increases, the phenomenon of stress concentration on this side gradually diminishes. Simultaneously, the stress gradually intensifies in the region opposite to the motion direction, reaching its peak value at 0.28 seconds.

2.2.2. Factors influencing thermal-mechanical coupling characteristics

According to the braking principle of monorail cranes, the axial fluctuation of the brake spring and the instability of high-pressure oil can both affect the braking force of the monorail crane.

As can be observed from Section 2.1, friction coefficient is a significant factor impacting the performance of thermal-mechanical coupling since the state of the brake shoe and track friction surface changes constantly.

The braking force is mainly provided by the frictional action of the brake shoes on both sides against the track surface. In theoretical analysis, it is usually assumed that the contact surface is a flat. However, in actual braking conditions, due to assembly errors, vibrations, and material wear, the friction area between the brake shoe and the track is smaller than the brake shoe area.

Thus, brake pressure, friction coefficient, initial speed and brake shoe area were selected as the influencing factors in this section. To investigate their effects on the temperature and stress fields of the monorail crane braking system during emergency braking, braking pressures of 13 MPa, 15MPa, 17MPa, and 19MPa, friction coefficients of 0.36, 0.38, 0.40, and 0.42, initial speed of 2.2m/s, 2.4m/s, 2.6m/s, and 2.8m/s, brake shoe radius of 32.5mm, 35mm, 37.5mm, and 40mm are selected for simulation.

2.2.3. Analysis of the variation trend of brake shoe in temperature and stress fields

Taking into account the temperature and stress differences at different locations on the brake shoe, as shown in Figure 7, the measuring point R was selected at the edge of the contact surface of the brake shoe.

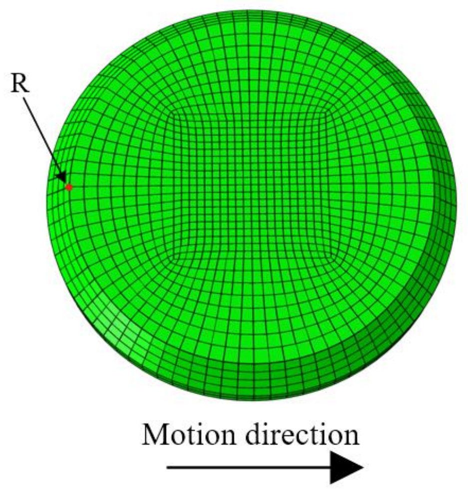

Fig. 7. Schematic diagram of measuring points.

From Figures 8 and 9, it can be seen that the changes in the temperature and stress fields of the brake shoe under different factors are roughly the same, showing a rising trend followed by a slow decline.

When other factors remain constant, increases in braking pressure, friction coefficient, initial speed all lead to higher temperatures and stress levels, while the brake shoe area has the opposite effect on them.

The analysis results also show that the more intense the friction between brake shoe and track, the longer the braking time, the larger the temperature and stress.

The FEA results of the above four factors on the thermal-mechanical coupling characteristics of the brake shoe are shown below:

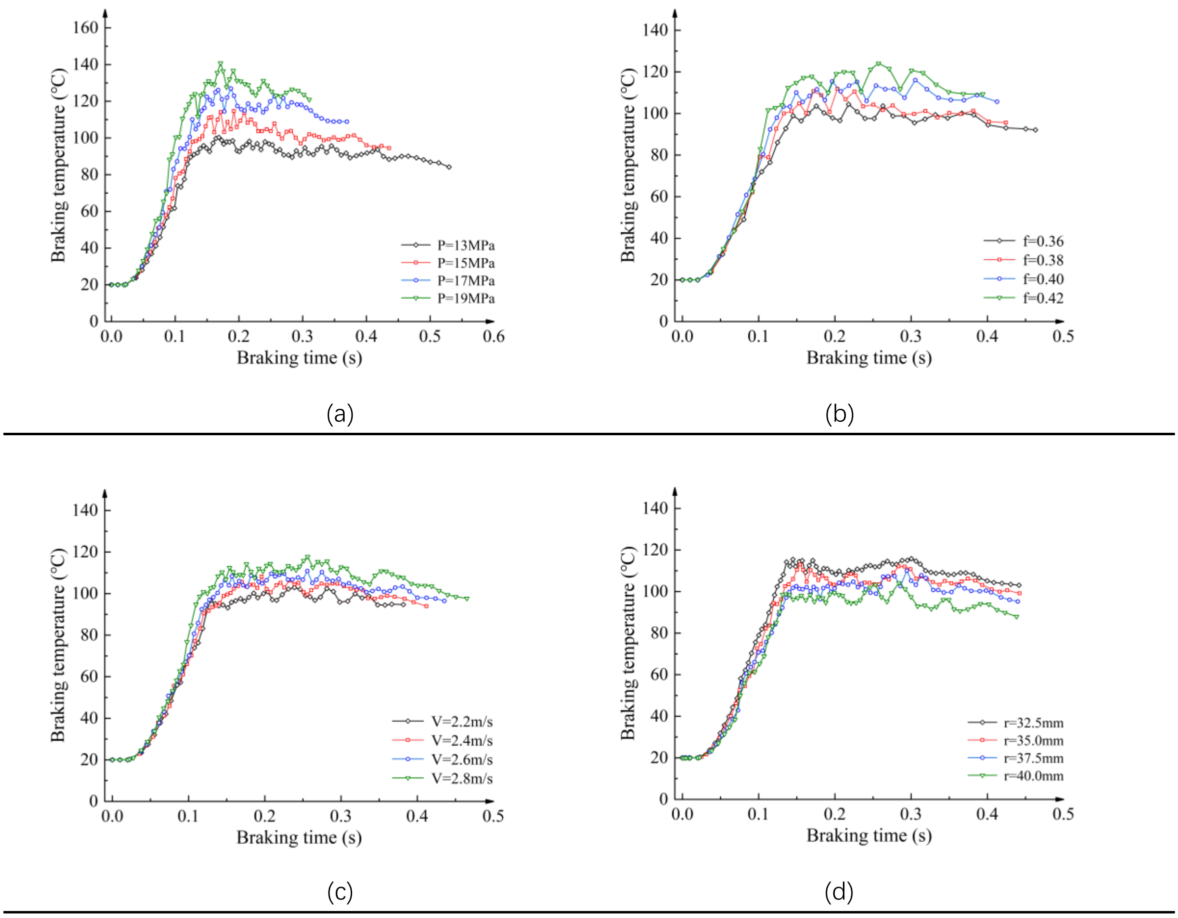

Fig. 8. Variation of brake shoe temperature for different factors.

(a) Braking temperature curve as brake pressure changes.

(b) Braking temperature curve as friction coefficient changes.

(c) Braking temperature curve as initial speed changes.

(d) Braking temperature curve as brake shoe area changes.

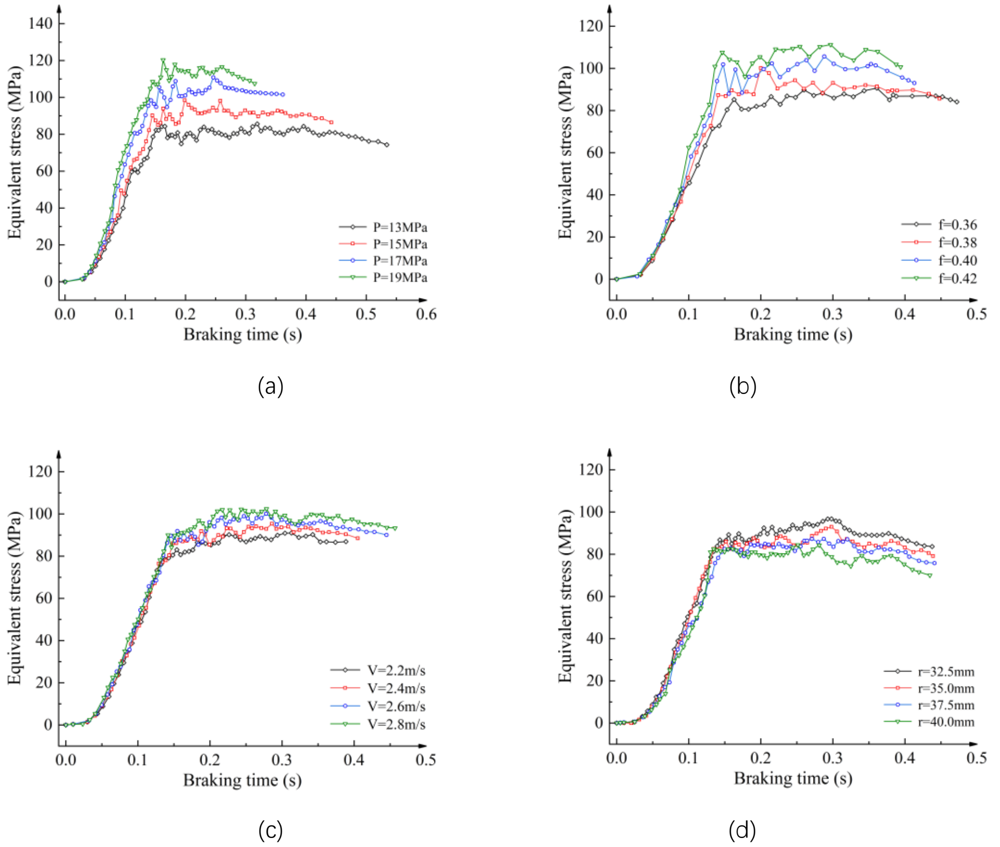

Fig. 9. Variation of brake shoe stress for different factors.

(a) Braking stress curve as brake pressure changes.

(b) Braking stress curve as friction coefficient changes.

(c) Braking stress curve curve as initial speed changes.

(d) Braking stress curve as brake shoe area changes.

3. Random response modeling of monorail crane emergency braking

When analyzing the braking performance of monorail cranes, parameters such as friction coefficient, braking pressure, and braking clearance are treated as constants. However, in real underground transportation environments, it is necessary to consider these parameters as random variables. Selecting the appropriate parameters and the variation of parameters is a foundation for reliability evaluation. The above FEA results can be used to determine parameters that have a significant impact on braking distance or temperature, while ignoring parameters that have little impact. In this section, a reliability response model was established with braking distance and braking temperature as response values.

3.1. Random response model based on DD

DD is a white-box model for classification, regression, and system identification, which can be used as a response model between random parameters and braking distance or braking temperature due to its high accuracy and low computational complexity [19].

The expression of DD is as follows:

$$Y = W^{L,L-1}[\cdots W^{l,l-1}(\cdots W^{21}(W^{10}X \circ X) \circ X \cdots) \circ X \cdots] \quad (1)$$

where X and Y denote the input and output spaces, L expresses the number of modules, $W^{l,l-1}$ is the weights matrix from the $(l-1)$th module to the l th module.

The forward propagation for DD module and linear module can be expressed as:

$$\begin{cases} A^l = W^{l,l-1}A^{l-1} \circ X \\ A^L = W^{L,L-1}A^{L-1} \end{cases} \quad (2)$$

The error backpropagation for DD module and linear module are shown as:

$$dA^L = \hat{Y} - Y \quad (3)$$

$$\begin{cases} dZ^L = dA^L \\ dZ^l = dA^l \circ X \end{cases} \tag{4}$$

$$dA^{l-1} = (W^{l,l-1})^T dZ^l \tag{5}$$

The weight adjustment equation of DD can be expressed as follows:

$$dW^{l,l-1} = \frac{1}{m} dZ^l (A^{l-1})^T \tag{6}$$

$$W^{l,l-1(new)} = W^{l,l-1(old)} - \alpha dW^{l,l-1} \tag{7}$$

where $\hat{Y}$ and Y are the outputs and labels of DD, respectively. m is the number of training samples, α is the learning rate that can be adapted with epochs.

3.2. Braking distance reliability modeling

The FEA results show that the small changes in spring stiffness, braking clearance, and friction coefficient all have a significant impact on braking performance. Assuming that the variables follow a normal distribution, the mean and standard deviation (SD) of these three parameters are given in Table 2.

Table 2. Mean and SD of random variables for braking distance.

Variables	Name	Mean	SD
R(N/mm)	Spring stiffness	1.46×10^2	4.29
f	Friction coefficient	0.38	1.12×10^{-2}
C(mm)	Braking clearance	10	5.9×10^{-1}

The above random variables were sampled in 80 groups by Latin Hypercube Sampling (LHS), of which 60 groups were used as training samples and 20 groups were used as test samples. The braking distance values of the 80 samples are obtained by ADAMS, and the sampling matrix is shown in Table A.1 in Appendix A.

The relationship between the braking distance of the monorail crane under emergency braking conditions and the random variables selected was obtained through a DD model, which can be expressed as

$$D = h(X_1) \tag{8}$$

where $X_1 = [R, f, C]^T$ is the vector of the random variables, D is the braking distance of the monorail crane.

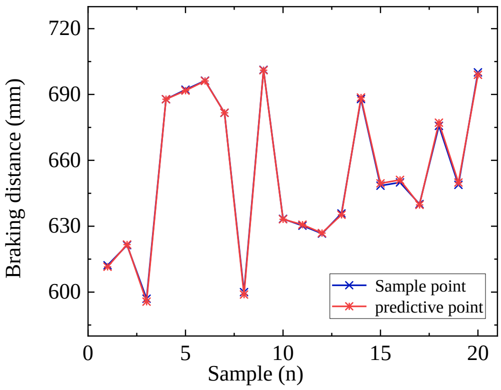

(a) Comparison between sample points and prediction points

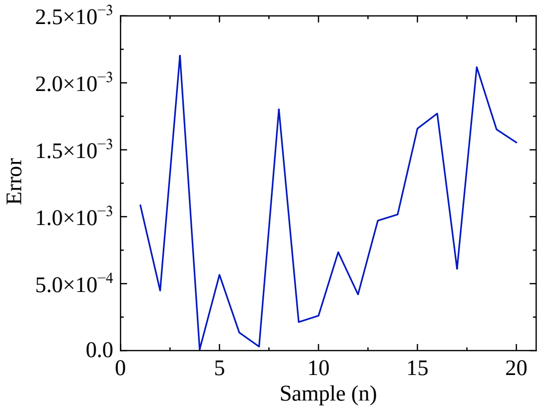

(b) Fitting relative error

Fig. 10. Comparison and fitting relative error of sample and prediction points.

A comparison of the sample points with the predicted points of the random response model is shown in Figure 10(a), and the relative fitting error is shown in Figure 10(b). The prediction points of the random response model based on the DD match the sample points well, and the relative fitting error is controlled within 1%. The results validate the accuracy of the DD, which can be used as an approximate substitute for the braking performance simulation of a monorail crane and to predict the braking distance.

3.3. Braking temperature reliability modeling

From the previous FEA results, the brake pressure, friction coefficient, and brake shoe area all have a significant effect on the braking temperature.

In addition to the above three factors, during the braking process of the monorail crane, a large amount of heat is generated by the friction between the brake shoe and the track. The elastic modulus of the material changes with temperature, so the elastic modulus is also chosen as a random variable. Since the braking force is mainly provided by the friction between the brake shoe and the track, as the braking time increases, the wear of the brake shoe surface results in changes in the thickness of the brake shoe. Therefore, the thickness of the brake shoe is chosen as another random variable.

In summary, the braking pressure, brake shoe area, friction coefficient, elastic modulus, and thickness of the brake shoe are selected as random variables in the analysis of the braking temperature reliability. Assuming that the variables follow a normal distribution, the mean and SD of these three parameters are given in Table 3. The random variables were sampled in 100 groups by LHS method, of which 80 groups were used as training samples and 20 groups were used as test samples. The braking temperature values of the 100 samples are obtained by ABAQUS, the sampling matrix is shown in Table A.2 in Appendix A.

Table 3. Mean and SD of random variables for braking temperature.

Variables	Name	Mean	SD
L(Pa)	Braking pressure	1.5×10^{7}	8.79×10^{5}
$S(m^2)$	Brake shoe area	3.87×10^{-3}	5.8×10^{-4}
f	Friction coefficient	0.38	2.2×10^{-2}
$E(\mathrm{N/m})^2$	Elastic modulus	1×10^{11}	5.86×10^{3}
$H(m)$	Thickness	0.01	5.27×10^{-4}

As in Section 3.1, the reliability performance function of the braking temperature is established using DD, as expressed in equation (9).

$$T = g(E, f, L, H, S) \tag{9}$$

where $X_2 = [E, f, L, H, S]^T$ is the vector of the random parameters, T is the braking temperature of the monorail crane.

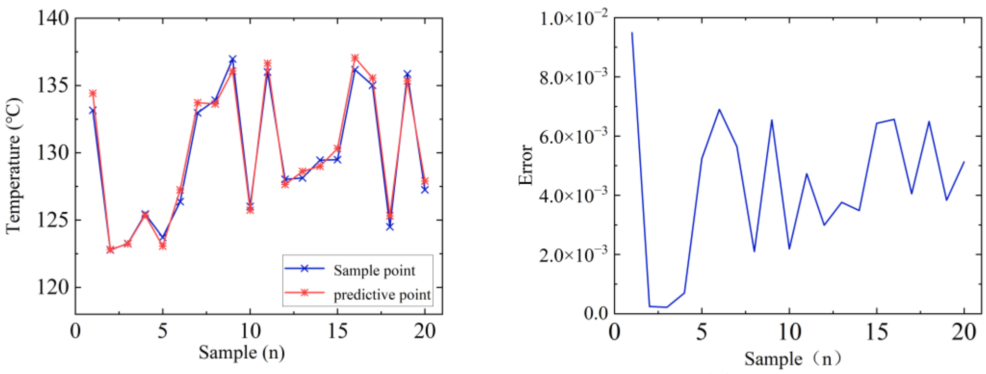

(a) Comparison between sample points and prediction points　（b）Fitting relative error

Fig. 11. Comparison and fitting relative error of sample and prediction points.

The comparison between the sample points and the predicted points of the random response model is shown in Figure 11 (a), and the relative fitting error is shown in Figure 11 (b). It can be seen that the relative fitting error is controlled within 1%. Therefore, DD can be used as an approximate substitute to FEA to predict the braking temperature.

4. Emergency braking performance reliability assessment of monorail cranes

4.1. High-order moment SPA method

Based on the results of random response modeling, this section applies the high-order moment SPA method to estimate the reliability of the braking system.

The high-order moment SPA method is proved to have high accuracy and efficiency [15,20]. Suppose that Y is a random variable with a probability density function (PDF), and its moment generating function (MGF) exists, expressed as $M_Y(t)$.

According to this method, the failure probability of the structure with the performance function $Y = g(x)$ can be expressed as

$$P_f = Pr(Y \leq 0) = Pr(Y_s \leq -\beta_2) = \Phi\left[\omega_y + \frac{1}{\omega_y} ln\left(\frac{v_y}{\omega_y}\right)\right] \tag{10}$$

where

$$\beta_2 = \frac{\mu_Y}{\sigma_Y} \tag{11}$$

$$\omega_y = sign(t_0)\sqrt{2[-\beta_2 t_0 - K_{Ys}(t_0)]} \tag{12}$$

$$v_y = t_0\sqrt{K_{Ys}''(t_0)} \tag{13}$$

K_{Ys} is the approximated CGF of the standardized variable Y_s, t_0 is the saddlepoint determined by the following equation:

$$t_0 = \left[\frac{\sqrt{(16a_2a_3+(\beta_2+a_1)^2)b^2+4a_2(\beta_2+a_1)b+4{a_2}^2}}{4ba_2} - \frac{(\beta_2+a_1)b+2a_2}{4ba_2}, \frac{-\sqrt{(16a_2a_3+(\beta_2+a_1)^2)b^2+4a_2(\beta_2+a_1)b+4{a_2}^2}}{4ba_2} - \frac{(\beta_2+a_1)b+2a_2}{4ba_2}\right] \tag{14}$$

$$a_1 = \frac{9\theta_{Ys}^3}{2(\eta_{Ys}-3)^2}, a_2 = \frac{-3\theta_{Ys}^3+2\eta_{Ys}-6}{4(\eta_{Ys}-3)}, a_3 = \frac{27\theta_{Ys}^4}{4(\eta_{Ys}-3)^3}, b = \frac{\eta_{Ys}-3}{3\theta_{Ys}} \tag{15}$$

When y=0, the estimated failure probability of the random structure is estimated at the mean of the Y=g(X) distribution, the CDF of the performance function is represented as:

$$F_Y(0) = Pr(Y_s \le 0) = \frac{1}{2} + \frac{K_Y'''(0)}{6\sqrt{2\pi}} \tag{16}$$

Therefore, when y=0, the estimated failure probability can be replaced by the following equation:

$$P_f = Pr(Y \le \mu_Y) = Pr(Y_s \le 0) = \frac{1}{2} + \frac{\theta_{Y_S}}{6\sqrt{2\pi}} \tag{17}$$

The detailed derivation process of the high-order moment SPA method can be found in our previous work [20].

4.2. Braking distance reliability calculation

According to the standards for the use of monorail cranes, the abrasion loss of the brake shoe must not exceed 15% of the original one, therefore the braking distance under the limit state of the shoes is regarded as the allowable value in this section. The performance function for the braking distance response of a monorail crane is modeled as:

$$h(Z) = D_0 - D \tag{18}$$

where $Z = [R, h, C]$ is the vector of the basic random variables; D_0 expresses the allowable value of braking distance; and D is the braking distance response with respect to the variables.

The failure probability of braking distance under emergency braking conditions can be obtained by using the high-order moment SPA method, which is 2.46×10^{-1} , and the reliability variation trend with braking distance allowable value is shown in Figure 12.

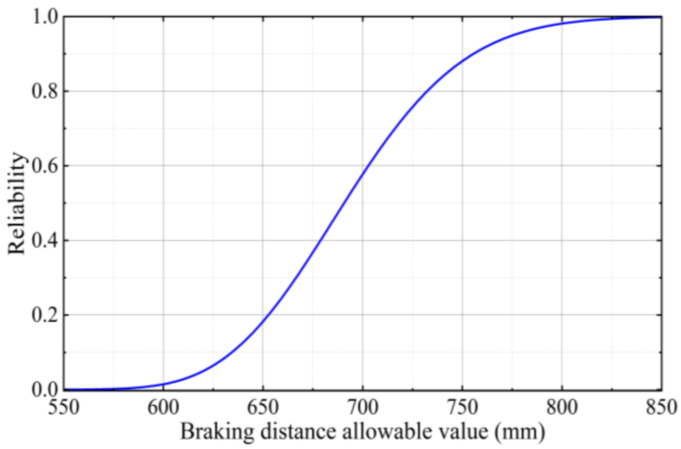

Fig. 12. Reliability curve with braking distance allowable value.

It can be seen from the reliability curve that the braking distance reliability increases with the increase of the braking distance allowable value. When the braking distance allowable value is below 691mm, the reliability is below 0.5. Under emergency braking conditions, if the reliability of the braking distance of the monorail crane is required to be no less than 0.9, the maximum braking distance cannot exceed 756mm.

4.3. Braking temperature reliability calculation

According to the safety requirements for underground equipment, the surface temperature of the brake shoe and track during the braking process cannot exceed 150 ℃, which is taken as the allowable value.

The performance function of the brake shoe temperature response is shown in the following equation:

$$g(\mathrm{X}) = T_0 - T \tag{19}$$

where $X = [L, S, f, E, H]$ is the vector of the random variables; T_0 is the braking temperature allowable value; T is the braking temperature response with respect to the variables.

The failure probability of the braking temperature under emergency braking conditions can be obtained as 3.652×10^{-2}, and the variation trend of reliability with braking temperature allowable value is shown in Figure 13.

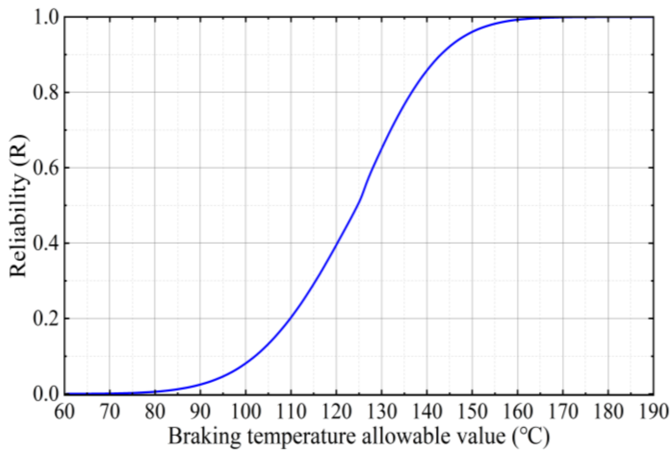

Fig. 13. Reliability curve with braking temperature allowable value.

The obtained reliability curve demonstrates that the reliability of braking temperature increases as the allowable value of braking temperature increases. When the failure temperature allowable value is below 80 ℃, the reliability of the brake shoe approaches zero. When the failure temperature allowable value is higher than 160 ℃, the reliability of the brake shoe approaches 1. When the failure temperature is within the range of 110 ℃~140 ℃, the reliability of the brake shoe varies greatly. In practice, if the reliability of the brake shoe is required to be no less than 0.9, the maximum temperature during the braking process cannot exceed 142.5 ℃.

5. Conclusions

In this work, the dynamic and thermal-mechanical coupling performance of monorail crane braking system was analyzed. Then, a random response model based on a DD was established, the high-order moment SPA method was applied to obtain the CDF of the performance function. Finally, the braking distance and temperature of the monorail crane braking system under failure threshold conditions were calculated. Some specific conclusions drawn from the present research are as follows:

(1) In the emergency braking process of monorail crane, long braking distance and braking time will lead to a high braking temperature, but too short braking distance will increase the braking risk. Therefore, a reasonable selection of relevant parameters is very important for braking safety.

(2) Taking the wear of the brake shoe up to 15% of the original size as the maximum braking distance allowable value, the probability of failure of the braking distance is 2.46×10^{-1}. Similarly, with a maximum allowable braking temperature of 150°C for the surface of the brake shoe, the probability of failure under emergency braking conditions is 3.652×10^{-2}.

Acknowledgments

The authors gratefully acknowledge the financial supports from National Natural Science Foundation of China (52375277, 52274155), the National Key Research and Development Program (2020YFB1314100) and a project funded by the Priority Academic Program Development of Jiangsu Higher Education Institutions (PAPD).

Appendix A

Table A.1. Sampling matrix of random variables of braking distance.

	R(N/mm) Spring stiffness	f Friction coefficient	C(mm) Braking clearance	D(mm) Braking distance
1	147.9591	0.361	10.797	737.0554
2	143.3363	0.36149	10.494	773.9713
3	143.7009	0.36195	9.38	739.4999
4	151.459	0.36244	9.051	662.4413
5	147.0258	0.36294	10.595	735.7056
6	140.565537	0.363394	9.684	775.4011
7	144.08004	0.363888	9.532	735.0493
8	148.134114	0.364382	10.241	712.6759
9	145.742502	0.364838	10.266	734.8992
10	142.971732	0.365332	10.165	758.0118
11	143.525886	0.365826	9.911	744.3565
12	140.200962	0.366282	10.722	801.1856
13	147.215385	0.366776	9.076	688.5523
14	153.1215	0.36727	9.886	655.0396
15	144.998769	0.367726	10.646	743.7126
16	141.863424	0.36822	9.278	738.3359
17	149.067426	0.368714	9.127	669.5709
18	149.986155	0.36917	9.43	667.0369
19	140.390541	0.369664	10.291	775.8421
20	151.094463	0.370158	9.557	658.4933
21	150.715305	0.370614	9.633	662.3117
22	146.471652	0.371108	9.329	690.6134
23	139.457229	0.371564	10.114	775.6653
24	145.917498	0.372058	9.962	707.7883
25	147.57996	0.372552	9.405	678.8576
26	151.269459	0.373008	9.177	642.9369
27	142.592574	0.373502	9.658	726.6531
28	149.606997	0.373996	9.785	666.6988
29	150.540309	0.374452	10.873	681.7682

30	151.823613	0.374946	10.139	653.799
31	142.782153	0.37544	10.823	749.685
32	139.282233	0.375896	11	790.4125
33	143.146728	0.37639	9.582	713.5011
34	138.903075	0.376884	9.861	759.7508
35	149.796576	0.37734	9.987	662.4782
36	138.5385	0.377834	9	738.0496
37	140.755116	0.378328	10.367	750.5655
38	152.756925	0.378784	10.747	650.6912
39	150.35073	0.379278	10.696	668.4529
40	142.053003	0.379772	10.013	725.4635
41	141.498849	0.380228	9.203	710.0456
42	139.092654	0.380722	10.519	765.8628
43	146.85081	0.381216	10.063	680.5898
44	147.769539	0.381672	10.443	679.7696
45	144.444615	0.382166	9.759	692.3471
46	148.877847	0.38266	10.544	670.5183
47	144.634194	0.383116	10.342	701.9684
48	148.688268	0.38361	9.481	647.3683
49	138.728079	0.384104	10.949	771.9439
50	144.80919	0.38456	10.19	693.6385
51	144.255036	0.385054	10.089	694.567
52	148.323693	0.385548	9.025	637.3896
53	152.567346	0.386004	10.038	623.5378
54	143.890461	0.386498	10.899	713.6368
55	145.363344	0.386992	10.468	689.545
56	146.296656	0.387448	9.734	664.6164
57	147.404964	0.387942	10.57	672.146
58	152.013192	0.388436	10.671	635.2209
59	140.011383	0.388892	10.848	743.7268
60	140.944695	0.389386	9.835	708.902
61	151.648617	0.389842	9.456	612.2098
62	152.377767	0.390336	10.316	621.3888
63	152.931921	0.39083	9.228	596.9782
64	141.30927	0.391286	9.253	687.8506
65	141.673845	0.39178	9.608	692.1675
66	139.836387	0.392274	9.152	696.2798
67	145.188348	0.39273	10.62	681.6544
68	152.202771	0.393224	9.354	599.9869
69	142.227999	0.393718	10.418	701.2223
70	150.161151	0.394174	10.392	633.3405
71	149.242422	0.394668	9.937	630.2452
72	148.513272	0.395162	9.506	626.6501
73	150.904884	0.395618	10.975	635.8212
74	139.646808	0.396112	9.101	687.9193
75	146.107077	0.396606	9.81	648.4648
76	145.552923	0.397062	9.709	649.93
77	149.432001	0.397556	10.772	640.1108
78	141.119691	0.39805	9.304	675.7188
79	146.661231	0.398506	10.215	648.8416
80	142.417578	0.399	10.924	700.0753

Table A.2. Sampling matrix of random variables of braking temperature.

	L(Pa) Braking pressure	S(m)^2 Brake shoe area	f Friction coefficient	E(N/m)^2 Elastic modulus	H(m) Thickness	T(°C) Temperature
1	14773000	0.003678	0.342	1.088×10^{11}	0.0109	118.6863
2	14561000	0.004018	0.34277	1.025×10^{11}	0.0102	114.5131
3	14409000	0.004142	0.34354	9.202×10^{10}	0.0108	117.2051
4	15470000	0.004246	0.3443	9.323×10^{10}	0.0103	117.8108
5	15045000	0.004787	0.34507	9.222×10^{10}	0.0097	117.5492

6	15288000	0.003897	0.34584	9.242×1010	0.0104	117.1419
7	15742000	0.003876	0.34661	9.626×1010	0.0100	120.3015
8	14833000	0.004480	0.34737	1.052×1011	0.0100	117.0961
9	13591000	0.004267	0.34814	9.121×1010	0.0096	112.2974
10	16197000	0.003373	0.34891	9.485×1010	0.0099	122.5822
11	13621000	0.003543	0.34968	9.808×1010	0.0107	116.4257
12	13803000	0.003718	0.35044	1.021×1011	0.0106	116.5205
13	16136000	0.002956	0.35121	9.000×1010	0.0093	124.6632
14	15591000	0.004588	0.35198	1.027×1011	0.0097	121.2418
15	14682000	0.003009	0.35275	9.707×1010	0.0101	117.0073
16	14864000	0.004162	0.35352	1.013×1011	0.0097	118.7736
17	16470000	0.003467	0.35428	1.072×1011	0.0093	127.8027
18	14318000	0.004039	0.35505	9.384×1010	0.0091	117.7228
19	14470000	0.004373	0.35582	1.092×1011	0.0099	117.7953
20	13500000	0.003957	0.35659	1.054×1011	0.0091	115.6199
21	15439000	0.003698	0.35735	9.364×1010	0.0098	120.8414
22	14076000	0.004809	0.35812	9.848×1010	0.0105	115.0407
23	15106000	0.003977	0.35889	1.007×1011	0.0105	123.0975
24	16227000	0.004437	0.35966	1.029×1011	0.0106	127.9205
25	14500000	0.004121	0.36042	9.545×1010	0.0104	116.7649
26	14197000	0.003659	0.36119	9.101×1010	0.0092	119.4532
27	13833000	0.003134	0.36196	1.096×1011	0.0097	113.7523
28	16379000	0.003797	0.36273	9.929×1010	0.0092	127.8197
29	15955000	0.002938	0.36349	1.086×1011	0.0096	124.4541
30	14955000	0.004204	0.36426	1.031×1011	0.0106	124.9628
31	14712000	0.003757	0.36503	9.343×1010	0.0108	122.0885
32	13864000	0.004610	0.3658	1.019×1011	0.0102	115.5858
33	15197000	0.003601	0.36657	9.040×1010	0.0108	124.2848
34	13652000	0.004676	0.36733	1.060×1011	0.0102	115.8841
35	15136000	0.003116	0.3681	1.076×1011	0.0098	122.1937
36	14136000	0.004632	0.36887	9.970×1010	0.0095	118.6828
37	15985000	0.003505	0.36964	1.094×1011	0.0102	125.7335
38	13985000	0.004183	0.3704	1.064×1011	0.0106	121.7786
39	16076000	0.003620	0.37117	1.056×1011	0.0107	129.8668
40	14015000	0.003261	0.37194	1.080×1011	0.0105	122.2707
41	14288000	0.003937	0.37271	9.505×1010	0.0100	118.7952
42	13712000	0.003817	0.37347	1.074×1011	0.0093	118.1187
43	16409000	0.004654	0.37424	1.070×1011	0.0104	128.2202
44	14621000	0.003737	0.37501	1.005×1011	0.0108	123.7097
45	15530000	0.003152	0.37578	9.586×1010	0.0092	126.4905
46	14652000	0.003777	0.37655	1.043×1011	0.0099	121.5512
47	14045000	0.004288	0.37731	1.009×1011	0.0095	120.2451
48	14924000	0.002921	0.37808	9.667×1010	0.0107	126.2723
49	13955000	0.003562	0.37885	1.023×1011	0.0095	119.614
50	14591000	0.003206	0.37962	1.017×1011	0.0106	124.56
51	16318000	0.003582	0.38038	1.068×1011	0.0101	129.1678
52	15894000	0.003317	0.38115	9.525×1010	0.0095	128.1855
53	15864000	0.003170	0.38192	9.646×1010	0.0104	128.3173
54	15561000	0.003391	0.38269	1.100×1011	0.0094	127.5502
55	15833000	0.003410	0.38345	9.020×1010	0.0098	126.99
56	15167000	0.004721	0.38422	1.078×1011	0.0096	125.9362
57	16439000	0.003354	0.38499	9.990×1010	0.0092	132.7185
58	15076000	0.004416	0.38576	9.424×1010	0.0100	124.1429
59	14227000	0.003026	0.38653	9.747×1010	0.0101	120.7883
60	13561000	0.003080	0.38729	1.084×1011	0.0107	122.3341
61	15682000	0.003188	0.38806	1.011×1011	0.0102	127.3176
62	16045000	0.003524	0.38883	1.001×1011	0.0101	129.1707
63	15409000	0.004567	0.3896	9.141×1010	0.0109	129.3616
64	14803000	0.003298	0.39036	9.889×1010	0.0091	127.4857
65	16288000	0.004854	0.39113	9.444×1010	0.0104	130.3736
66	14379000	0.004523	0.3919	9.404×1010	0.0092	124.1892
67	15348000	0.004743	0.39267	1.062×1011	0.0098	128.869

68	15379000	0.002974	0.39343	9.283×1010	0.0092	130.876
69	15318000	0.004459	0.3942	1.066×1011	0.0101	127.4359
70	14985000	0.004765	0.39497	9.606×1010	0.0096	125.7334
71	15015000	0.004352	0.39574	9.828×1010	0.0103	125.447
72	14258000	0.003639	0.39651	9.465×1010	0.0105	122.376
73	16500000	0.003243	0.39727	9.687×1010	0.0095	133.7173
74	16015000	0.004394	0.39804	1.039×1011	0.0097	131.5063
75	13773000	0.003486	0.39881	1.098×1011	0.0096	122.1385
76	15773000	0.004502	0.39958	9.162×1010	0.0094	132.2778
77	16258000	0.004545	0.40034	1.041×1011	0.0100	136.1559
78	16106000	0.003998	0.40111	1.033×1011	0.0097	134.9299
79	15500000	0.003062	0.40188	1.047×1011	0.0102	129.0594
80	15652000	0.004059	0.40265	1.045×1011	0.0108	134.7827
81	16167000	0.003837	0.40341	1.082×1011	0.0099	133.1559
82	14167000	0.004899	0.40418	9.566×1010	0.0103	122.7866
83	13924000	0.004309	0.40495	1.058×1011	0.0104	123.2606
84	13530000	0.004698	0.40572	9.081×1010	0.0096	125.4599
85	13742000	0.004225	0.40648	1.015×1011	0.0094	123.7138
86	14530000	0.003856	0.40725	9.303×1010	0.0099	126.3789
87	15803000	0.003280	0.40802	9.182×1010	0.0094	132.9724
88	16348000	0.003335	0.40879	9.727×1010	0.0103	133.914
89	15924000	0.003917	0.40956	9.768×1010	0.0105	136.9755
90	13682000	0.003429	0.41032	9.788×1010	0.0108	126.0202
91	15621000	0.004832	0.41109	1.035×1011	0.0107	136.0094
92	14742000	0.004100	0.41186	1.090×1011	0.0103	128.0293
93	14348000	0.002991	0.41263	1.037×1011	0.0094	128.136
94	14439000	0.003224	0.41339	9.909×1010	0.0093	129.4523
95	14894000	0.003044	0.41416	9.061×1010	0.0098	129.4947
96	15712000	0.003448	0.41493	9.949×1010	0.0108	136.1698
97	15258000	0.004877	0.4157	1.049×1011	0.0093	135.0112
98	13894000	0.003098	0.41646	1.003×1011	0.0100	124.5048
99	15227000	0.00408	0.41723	9.869×1010	0.0106	135.8654
100	14106000	0.00433	0.418	9.263×1010	0.0094	127.2536

Reference

1. Blatman G, Sudret B. An adaptive algorithm to build up sparse polynomial chaos expansions for stochastic finite element analysis. Probabilistic Engineering Mechanics 2010; 25(2): 183-197, https://doi.org/10.1016/j.strusafe.2019.101905.
2. Cheng K, Lu Z Z. Structural reliability analysis based on ensemble learning of surrogate models. Structural Safty 2020; 83: 101905, https://doi.org/10.1016/j.strusafe.2019.101905.
3. Dammak K, Baklouti A, El Hami A. Optimal reliable design of brake disk using a Kriging surrogate model. Mechanics of Advanced Materials and Structures 2022; 29(28):7569-7578, https://doi.org/10.1080/15376494.2021.2002983.
4. Deng J, Gu D S, Li X B, Yue Z Q. Structural reliability analysis for implicit performance functions using artificial neural network. Structural Safety 2005; 27(1): 25-48, https://doi.org/10.1016/j.ijsolstr.2005.05.055.
5. Du X P, Sudjianto A. First-order saddlepoint approximation for reliability analysis. Aiaa Journal 2004; 42(6): 1199-1207, https://doi.org/10.2514/1.3877.
6. Du X P. System reliability analysis with saddlepoint approximation. Structural and Multidisciplinary Optimization 2010; 42(2): 193-208, https://doi.org/10.1007/s00158-009-0478-x.
7. Echard B, Gayton N, Lemaire M. AK-MCS: An active learning reliability method combining Kriging and Monte Carlo Simulation. Structural Safety 2011; 33(2): 145-154, https://doi.org/10.1016/j.strusafe.2011.01.002.
8. Forrester A I J, Keane A J. Recent advances in surrogate-based optimization. Progress in Aerospace Sciences 2009; 45(1-3): 50-79, https://doi.org/10.1016/j.paerosci.2008.11.001.
9. Gogu C, Passieux J C. Efficient surrogate construction by combining response surface methodology and reduced order modeling. Structural and Multidisciplinary Optimization 2013; 47(6): 821-837, https://doi.org/10.1007/s00158-012-0859-4.
10. Guo S X. An efficient third-moment saddlepoint approximation for probabilistic uncertainty analysis and reliability evaluation of structures.

Applied Mathematical Modelling 2014; 38(1): 221-232, https://doi.org/10.1016/j.apm.2013.06.026.
11. Guo Y Q, Lv Z Y. An uncertainty analysis and reliability-based multidisciplinary design optimization method using fourth-moment saddlepoint approximation. Cmes-Computer Modeling in Engineering & Sciences 2023; 134(3): 1855-1870, https://doi.org/10.32604/cmes.2022.022211.
12. Guo Z, Bai G. Application of Least Squares Support Vector Machine for Regression to Reliability Analysis. Chinese Journal of Aeronautics 2009; 22(2): 160-166, https://doi.org/10.1016/S1000-9361(08)60082-5.
13. Hu Z, Nannapaneni S; Mahadevan S. Efficient Kriging surrogate modeling approach for system reliability analysis. AI EDAM-Artificial Intelligence for Engineering Design Analysis and Manufacturing 2017; 31(2): 143-160, https://doi.org/10.1017/S089006041700004X.
14. Huang B Q, Du X P. Uncertainty analysis by dimension reduction integration and saddlepoint aporoximations. Journal of Mechanical Design 2006; 128(1): 26-33, https://doi.org/10.1115/1.2118667.
15. Huang X Z, Liu Y, Zhang Y M, Zhang X F. Reliability analysis of structures using stochastic response surface method and saddlepoint approximation. Structural and Multidisciplinary Optimization 2017; 55(6): 2003-2012, https://doi.org/10.1007/s00158-016-1617-9.
16. Huang X Z, Zhang Y M. Reliability-sensitivity analysis using dimension reduction methods and saddlepoint approximations. International Journal for Numerical Methods in Engineering 2013; 93(8): 857-886, https://doi.org/10.1002/nme.4412.
17. Kaymaz I. Application of kriging method to structural reliability problems.Structural Safety 2005; 27(2): 133-151, https://doi.org/10.1016/j.strusafe.2004.09.001.
18. Li H S. Reliability-based design optimization via high order response surface method. Journal of Mechanical Science and Technology 2013; 27(4): 1021-1029, https://doi.org/10.1007/s12206-013-0227-3.
19. Liu G, Wang J. Dendrite net: a white-box module for classification, regression, and system identification. Ieee Transactions on Cybernetics 2021; 52(12): 13774-13787, https://doi.org/10.1109/TCYB.2021.3124328.
20. Lu H, Cao S, Zhu Z C, Zhang Y M. An improved high order moment-based saddlepoint approximation method for reliability analysis. Applied Mathematical Modelling 2020; 82: 836-847, https://doi.org/10.1016/j.apm.2020.02.006.
21. Lyu H, Shangguan W B, Yu D J. A unified approach for squeal instability analysis of disc brakes with two types of random-fuzzy uncertainties. Mechanical Systems and Signal Processing 2017; 93:281-298, https://doi.org/10.1016/j.ymssp.2017.02.012.
22. Lyu H, Yu D J. Brake squeal reduction of vehicle disc brake system with interval parameters by uncertain optimization. Journal of Sound and Vibration 2014; 333(26): 7313-7325, https://doi.org/10.1016/j.jsv.2014.08.027.
23. Marelli S, Sudret B. An active-learning algorithm that combines sparse polynomial chaos expansions and bootstrap for structural reliability analysis. Structural Safety 2018; 75: 67-74, https://doi.org/10.1016/j.strusafe.2018.06.003.
24. Ren C, Aoues Y, Lemosse D, De Cursi. Ensemble of surrogates combining Kriging and Artificial Neural Networks for reliability analysis with local goodness measurement. Structural Safety 2022; 96:102186, https://doi.org/10.1016/j.strusafe.2022.102186.
25. Ren F B, Chen G A, Lu H, Cao S. The probabilistic modeling and reliability analysis of brake shoes for hoist disc brake with correlated failure modes. Advances in Mechanical Engineering 2020; 12(6):1-12, https://doi.org/10.1177/1687814020934596.
26. Tvedt L. Second Order Reliability by an Exact Integral. Berlin, Heidelberg, Springer Berlin Heidelberg:1989. https://doi.org/10.1007/978-3-642-83828-6_26
27. Xiang Z, Chen J, Bao Y, Li H. An active learning method combining deep neural network and weighted sampling for structural reliability analysis. Mechanical Systems and Signal Processing 2020; 140:106684, https://doi.org/10.1016/j.ymssp.2020.106684.
28. Yang Z, Pak U, Kwon C, Zhang Y M. A reliability-based robust optimization design for the drum brake using adaptive Kriging surrogate model. Quality and Reliability Engineering International 2023; 39(1): 454-471, https://doi.org/10.1002/qre.3230.
29. Yang Z, Pak U, Kwon C. Vibration reliability analysis of drum brake using the artificial neural network and important sampling method. Complexity 2021, https://doi.org/10.1155/2021/5517634.
30. Yang Z, Pak U, Yan Y, Kwon C. Reliability-Based Robust Optimization Design for vehicle drum brake considering multiple failure modes. Structural and Multidisciplinary Optimization 2022;65(9):229-246, https://doi.org/10.1007/s00158-022-03349-z.
31. Yuan R, Meng, D B, Li, H Q. Multidisciplinary reliability design optimization using an enhanced saddlepoint approximation in the framework of sequential optimization and reliability analysis. Proceedings of The Institution of Mechanical Engineers Part O-Journal of Risk and Reliability 2017; 230(6): 570-578, https://doi.org/10.1177/1748006X16673500.

32. Zhang N, Jiang G J, Wu D W, Chen H X, Wu J X. Fatigue reliability analysis of the brake pads considering strength degradation. Eksploatacja I Niezawodnosc-Maintenance and Reliability 2020; 22(4): 620-626, https://doi.org/10.17531/ein.2020.4.5.
33. Zhou Q Y, Li Z L, Fan W L, Ang A H S, Liu R Y. System reliability assessment of deteriorating structures subjected to time-invariant loads based on improved moment method. Structural Safety 2017; 68: 54-64, https://doi.org/10.1016/j.strusafe.2017.05.006.
34. Zhou Y C, Lu Z Z. An enhanced Kriging surrogate modeling technique for high-dimensional problems. Mechanical Systems and Signal Processing 2020; 140: 106687, https://doi.org/10.1016/j.ymssp.2020.106687.